ISSN 1063-7729, Astronomy Reports, 2006, Vol. 50, No. 3, pp. 167–181. © Pleiades Publishing, Inc., 2006.
Original Russian Text © A.S. Gusev, 2006, published in Astronomicheskiĭ Zhurnal, 2006, Vol. 83, No. 3, pp. 195–210.

Multicolor CCD Photometry of Six Lenticular and Spiral Galaxies. Structure of the Galaxies

A. S. Gusev

Sternberg Astronomical Institute, Universitetskiĭ pr. 13, Moscow, 119992 Russia

Received April 18, 2005; in final form, September 7, 2005

Abstract—The results of multicolor surface photometry of the S0 galaxies NGC 524, NGC 1138, and NGC 7280 and the spiral galaxies NGC 532, NGC 783, and NGC 1589 are reported. $UBVRI$ observations were acquired with the 1.5-m telescope of the Maidanak Observatory (Uzbekistan), while JHK data were taken from the 2MASS catalog. The overall structure of the galaxies is analyzed and the galaxy images decomposed into bulge and disk components. The parameters of the galaxy components—rings, bars, spiral arms, and dust lanes—are determined. The bulge/disk decompositions based on averaged one-dimensional photometric profiles yield incorrect parameters for the bulges of the S0–Sa galaxies with bars and/or rings, whose inner regions are dominated by the radiation of the bulge.

PACS numbers : 98.52.L, 98.52.N
DOI: 10.1134/S1063772906030012

1. INTRODUCTION

This work is a part of an extensive program of studies of the physical (photometric and kinematic) properties of S0 galaxies and their comparison with the parameters of spiral galaxies. S0 galaxies are similar in structure to spiral galaxies but display a lack of gas. The origin of S0 galaxies remains an open question: several possible mechanisms for the rapid depletion of gas in lenticular galaxies have been discussed. Information about the stability of the stellar disks of S0 galaxies and the contribution of dark matter to the total mass of the galaxies may provide important insights into the evolution of S0 galaxies. This requires knowledge of both kinematic and photometric parameters. In this paper, we analyze visible and near-IR photometric data for six lenticular and spiral galaxies. Surface photometry obtained over a wide wavelength interval can be used to determine the structure and composition of the stellar populations of galaxies. We pay special attention to identifying "flat" components in lenticular and spiral galaxies and studying the specific features of their structure and radial gradients of the age and chemical composition of the stellar population. The first part of this paper analyzes the overall structure of the galaxies, and the parameters of their disks and bulges. We use the "mask" method (subtraction of the disk and bulge brightness distributions from the overall brightness distribution of the galaxy) to analyze the characteristic features of the morphologies of the galaxies. The second part of the paper considers the $UBVRIJHK$ photometric properties of the galaxies and the composition of their stellar populations.

2. BASIC INFORMATION ABOUT THE GALAXIES

We chose early-type (S0-Sab) galaxies (the only exception is the Sc galaxy NGC 783) with sufficiently high luminosities ($M_B^{0,i} < -19.4^m$) for our study. Our sample represents systems with different inclinations (from the almost face-on galaxy NGC 524 to the strongly inclined galaxies NGC 532 and NGC 1589). We chose galaxies with angular diameters not exceeding $3.5'$, due to the size of our CCD images, $8.9' \times 3.6'$.

Most of the program galaxies are poorly studied objects. We were the first to perform multicolor (more than four-band) surface photometry of NGC 532, NGC 783, and NGC 1138. Table 1 summarizes the main parameters of the galaxies adopted from the LEDA database.

Let us now discuss each of the galaxies studied in more detail.

NGC 524. This is a well-known giant lenticular galaxy viewed almost face-on. It is the center of a group of 8–14 galaxies [4].

Numerous photometric and spectroscopic observations have been obtained for this galaxy [3, 5–13]. The galaxy exhibits an excess metallicity in its central region [11, 13], and the nucleus is richer in heavy

Table 1. Main parameters of the galaxies (according to the LEDA database)

Parameter	NGC 524	NGC 532	NGC 783	NGC 1138	NGC 1589	NGC 7280
Type (NED)	SA(rs)0+	Sab?	S(B)c	SB0	Sab	SAB(r)0+
Type (LEDA)	−1.2	2.0	5.1	−2.1	1.8	−1.0
m_B, mag	11.46	14.08	13.85	13.85	12.85	13.07
$M_B^{0,i}$, mag	−21.63	−19.48	−21.14	−19.57	−21.73	−19.41
$V_{\rm Vir}$, km/s	2429	2364	5290	2470	3712	1942
R, Mpc	32.4	31.5	70.5	32.9	49.5	25.9
D_{25}, arcmin	3.31	3.31	1.58	1.55	3.16	2.09
D_{25}^0, kpc	33.4	31.6	33.3	17.5	47.7	16.2
i, deg	8.4	75.6	49.2	32.0	84.7	53.9
b/a	1.00	0.37	0.68	0.89	0.31	0.68
PA, deg	–	32.0	60.5	79.0	159.4	76.0
$V_{\rm max}$, km/s	–	191	46	25 [1]	323	131
σ_0, km/s	252	124	–	145 [1]	200	104
$A_B^{\rm gal}$, mag	0.36	0.40	0.26	0.65	0.37	0.24
$(U-B)_0^i$, mag	0.52	0.56	–	–	0.32	0.34
$(B-V)_0^i$, mag	0.95	0.83	–	–	0.84	0.82
$(V-R)_0^i$, mag	0.62 [2]	–	–	–	–	0.56 [2]
$(V-I)_0^i$, mag	1.22 [3]	–	–	–	1.03	1.16

elements than the bulge [11]. According to Hα observations, the galaxy bears the marks of nuclear activity, and is classified as an intermediate-type object between LINERS and HII galaxies [41].

NGC 524 has a stellar disk with a radius of $4''-5''$ [11], a gaseous disk with a radius of up to $20''$ inclined to the plane of the galaxy [11], and dust rings and lines at galactocentric distances of $5''$ [6], $\sim 10''-15''$ [8, 15], and $40''$ [5]. Baggett et al. [7] and Kent [9, 10] performed a bulge/disk decomposition for this galaxy.

NGC 524 has normal X-ray and IR parameters (see, e.g., [8, 16, 17]). The dust mass in the galaxy is estimated to be $(1-6)\times 10^5\,M_\odot$ [8, 17]. The mass of neutral hydrogen does not exceed $(4-5)\times 10^8\,M_\odot$ [18]. The mass of HII is $4.5\times 10^3\,M_\odot$, and the size of the HII emission region is $40''\times 40''$ [19].

A study of almost 500 globular clusters in NGC 524 yielded an estimate for the total mass of the galaxy of $(4-13)\times 10^{11}\,M_\odot$ [12].

NGC 532. This strongly inclined early-type spiral galaxy belongs to the NGC 524 group [4]. $BVRI$ photometry was performed earlier in order to study the morphological features and determine the geometrical parameters (the ellipticity and position angle of isophotes) of NGC 532 [20, 21]. Prugniel et al. [22] analyzed the kinematics of the galaxy based on spectroscopic observations. Determinations of the position angle ($\mathrm{PA}=28^\circ-32^\circ$) and inclination ($i=75^\circ-80^\circ$) of the galaxy by various authors are in good agreement.

Lutticke et al. [23] pointed out the asymmetry of the bulge of NGC 532: on one side, the bulge isophotes have a rectangular ("boxy") shape, while they have an oval shape on the other side. Lu [21] decomposed the brightness distribution of the galaxy into bulge and disk contributions.

The galaxy is fairly rich in gas ($M_{\rm HI}=1.6\times 10^9\,M_\odot$) [24]. The mass of dust $M_{\rm dust}$ was estimated to be $3.3\times 10^6\,M_\odot$ [24].

The X-ray and IR luminosities of NGC 532 are typical for galaxies of the corresponding morphological type and optical luminosity [16].

NGC 783. This is a late-type galaxy with numerous star-forming regions. It is also known as IC 1765, and is listed in the Markarian catalog galaxies (Mrk 1171). Moriondo et al. [25] determined the

position angle and inclination based on H-band photometric observations. Contini et al. [26] analyzed the blue nucleus of NGC 783 and its two brightest HII regions using spectroscopic data and BVR photometry.

The galaxy is rich in dust ($M_{\rm dust} = 2.6 \times 10^7\,M_\odot$) [27]. Analysis of IR data at wavelengths $12-100\,\mu$m shows a predominance of cold dust in the disk [25]. The total IR luminosity of the galaxy is $(1-2) \times 10^{10}\ L_\odot$ [27], and the mass of neutral hydrogen is $M_{\rm HI} = (1.0 \pm 0.5) \times 10^{10}\,M_\odot$ [27].

NGC 1138. This is a typical barred lenticular galaxy viewed face on. It has not been studied before except for spectroscopic observations by Simien and Prugniel [1]. All the available data for this galaxy are listed in Table 1.

NGC 1589. This is an early-type, strongly inclined, giant spiral galaxy with a powerful double dust disk. $BVRI$ [20] and UBV [17] surface photometry has been performed in order to study its structural features. The groups of Kuchinski and Jansen used $UBVRIJHK$ photometry to study the distribution and properties of the dust in NGC 1589 [28–30]. The V-band extinction, A_V, in the nearly edge-on dust disk is $0.9^m-1.5^m$ [28], the K-band extinction $A_K = 0.20^m-0.24^m$ [29], and the total extinction ("extinction due to the inclination of the galaxy") $0.5^m-1.0^m$ in V [30]. The photometric data do not enable unambiguous choice of a particular model for the dust distribution in NGC 1589 (a "screen of dust" or dust uniformly mixed with the stars) [28–30]. Jansen et al. [28] identify three dust lanes along the major axis and explain their triplicity as a geometrical effect due to the projection of the spiral arm onto the dust disk.

The powerful dust disk distorts the shapes of the galactic isophotes. The isophotes of both the bulge [23, 31] and the entire galaxy have boxy shapes. Lutticke et al. [31] classify the bulge of NGC 1589 as a "thick boxy bulge" with the brightness decrease law $I \sim r^{-1/2}$. According to [31], such bulges form during relatively late stages of a galaxy's evolution. This hypothesis is supported by the data of Jablonka et al. [13], who studied the chemical composition of the bulge. Lutticke et al. [31] also suspect that NGC 1589 has a bar [31].

The dust lanes indicate the inclination of the galaxy only rather crudely: the inferred i values range from 69° to 85° [28]. Kent [9, 10] decomposed the brightness profile of the galaxy into bulge (with its brightness decreasing according to a de Vaucouleurs law) and disk components [9, 10].

Despite the apparent manifestations of dust in NGC 1589, the IR luminosity of this galaxy is rather low ($L_{\rm FIR} = 1.9 \times 10^9\ L_\odot$) [17], and the mass of dust is estimated to be $1.3 \times 10^6\,M_\odot$ [17]. The mass of neutral hydrogen in NGC 1589 is $M_{\rm HI} = 5.5 \times 10^9\,M_\odot$ [17].

NGC 7280. This is an SB0a galaxy with a complex multicomponent structure in its central region. It has been well studied, and surface photometry in various filters is available [21, 32–35]. Afanasiev and Sil'chenko [35] performed spectrophotometric studies of the nucleus of NGC 7280, and Caldwell et al. [36] performed spectrophotometry of the entire galaxy. The galaxy has a well-defined, young ($\sim 1.5 \times 10^{10}$ yr), chemically distinct nucleus [35] whose angular size is of the order of 1″ [35]. It contains a strongly inclined inner stellar disk (according to Afanasiev and Sil'chenko [35]) or a bar (according to Erwin and Sparke [34]) with PA ≈ 110° and a diameter of 2″–3″. The circumnuclear region also hosts a gaseous disk [35] (which Erwin and Sparke [34] interpret as a ring) orthogonal to the main stellar disk of the galaxy. There are also numerous dust lanes with complex configurations located within 7″ to the west of the center [34], and a long dust lane 23″ to the east of the center [34]. The galaxy also exhibits a classical bar with a radius of 27″ and PA = 55° [34, 37]. The complex central structure of NGC 7280 may be due to its interaction with a faint Irr companion galaxy located 4.2′ to the northeast of NGC 7280 [34, 35].

The bulge/disk decompositions of the brightness distribution of NGC 7280 derived by Lu [21], Alonso et al. [32], and de Souza et al. [33] agree poorly with each other. For example, Alonso et al. [32] and de Souza et al. [33] find the bulge-to-disk R-band luminosity ratio to be 0.5 and 3.0, respectively.

The mass of neutral hydrogen in the galaxy is $M_{\rm HI} = (1-5) \times 10^8\,M_\odot$ (see, e.g., [24, 38]), and the mass of dust is estimated to be $5.6 \times 10^4\,M_\odot$ [24], despite the numerous dust lanes in the central part of the galaxy. Van Driel and van Woerden [38] estimated a lower limit for the total mass of NGC 7280 of $2 \times 10^{10}\,M_\odot$.

3. OBSERVATIONS AND DATA REDUCTION

We observed the six galaxies in November 2003 with the SIT-2000 CCD mounted on the 1.5-m telescope of Maidanak Observatory of the Ulugh-Bek Institute of Astronomy of the Academy of Sciences of the Republic of Uzbekistan (with a focal distance of 12 m). When combined with the U, B, V, R, and I filters, this CCD realizes a photometric system that is close to the standard Johnson–Cousins $UBVRI$ system. Data about the filters used can be found in [39]. The CCD was cooled using liquid nitrogen. The size of the CCD was 2000×800 pixels, which provides a field of view of $8.9' \times 3.6'$ for an image scale

Table 2. Observation log

Date	Galaxy	Filter	Exposures, s	Air mass	Seeing
November 17/18, 2003	NGC 532	U	3×300	1.16	1.6″
		B	$2 \times 300, 240$	1.15	1.8
		V	$2 \times 240, 210$	1.15	1.8
		R	3×180	1.15	1.5
		I	3×120	1.15	1.2
	NGC 7280	U	3×300	1.25	2.1
		B	3×300	1.20	1.9
		V	$2 \times 240, 210$	1.15	1.7
		R	$2 \times 210, 180$	1.12	1.7
		I	3×180	1.11	1.8
November 18/19, 2003	NGC 524	U	3×300	1.21	1.7
		B	$2 \times 300, 240$	1.18	1.2
		V	3×180	1.17	0.9
		R	3×120	1.14	0.8
		I	$2 \times 90, 120$	1.15	0.9
	NGC 1138	U	3×300	1.07	1.8
		B	3×300	1.05	1.4
		V	$2 \times 240, 210$	1.01	1.4
		R	$2 \times 150, 120$	1.01	1.2
		I	$2 \times 90, 120$	1.00	1.1
November 24/25, 2003	NGC 783	U	3×300	1.09	1.0
		B	2×300	1.07	1.0
		V	2×240	1.05	0.8
		R	2×180	1.04	0.8
		I	2×120	1.04	0.7
	NGC 1589	U	3×300	1.30	1.3
		B	2×300	1.28	1.0
		V	2×240	1.27	0.8
		R	2×180	1.27	0.8
		I	$90, 120$	1.27	0.7

of 0.267″/pixels × 0.267″/pixels. Table 2 gives a log of the observations.

We carried out the further reduction of the CCD images at the Sternberg Astronomical Institute using the standard procedure and the ESO–MIDAS image-reduction system. The main stages of the reduction included bias subtraction and flat-fielding, removal of cosmic-ray traces, determining and subtracting the sky background for each image, matching the galaxy images using reference stars, co-adding galaxy images made in the same filter, transforming the counts to a logarithmic scale (magnitudes per square arcsec) based on the results of the photometric calibration, correcting the deviation of the instrumental photometric system from the

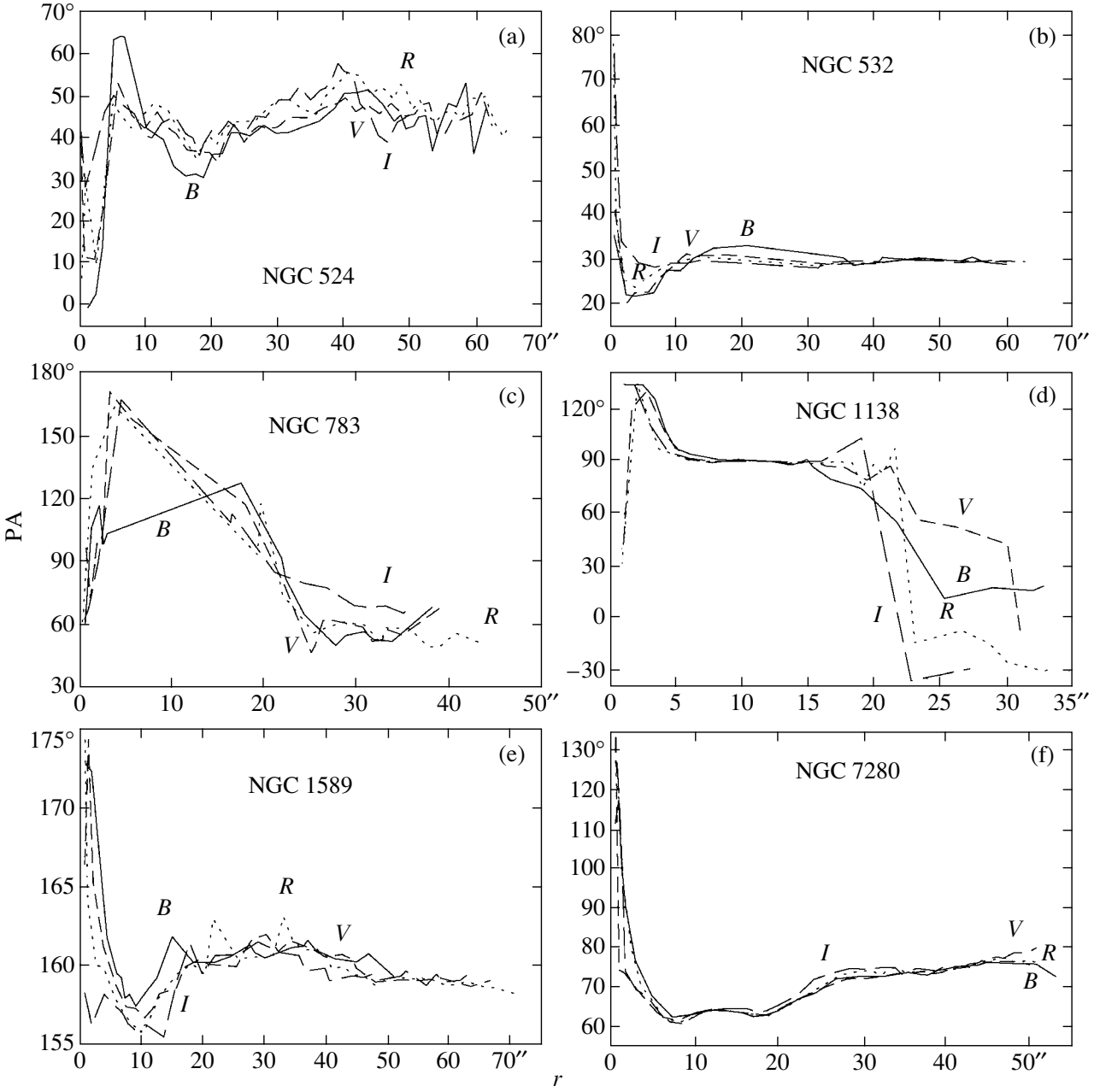

Fig. 1. Dependence of the position angle, PA, on galactocentric distance r for (a) NGC 524, (b) NGC 532, (c) NGC 783, (d) NGC 1138, (e) NGC 1589, and (f) NGC 7280 in the B (solid), V (short-dashed), R (dotted), and I (long-dashed) filters.

standard Johnson–Cousins system, correcting for the air mass (with allowance for the derived color equations and the aperture photometry of galaxies), and subtracting the galaxy images taken in different filters to construct color-index maps.

We used observations of the Landolt standard stars RU 149, PG 1047+003, PG 2336+004, SA 95, and SA 98 [40] and the open cluster NGC 7790 [41] taken on the same nights in the U, B, V, R, and I filters in the air-mass interval $M(z) \equiv \sec z = 1.1-1.9$ to derive the color equations and correct for atmospheric extinction. We obtained $UBVRI$ photometry for 88 stars and measured the fluxes of 65 stars at different $M(z)$ values. The resulting instrumental $ubvri$ system was close to the standard Johnson–Cousins $UBVRI$ photometric system, with accuracies of better than 0.02^m in the B, V, R, and I bands and 0.04^m in the U [39] band.

We also compared the data obtained for NGC 524, NGC 532, NGC 1589, and NGC 7280 with the results of aperture photometry (from the HyperLEDA electronic catalog). The accuracy of the photomet-

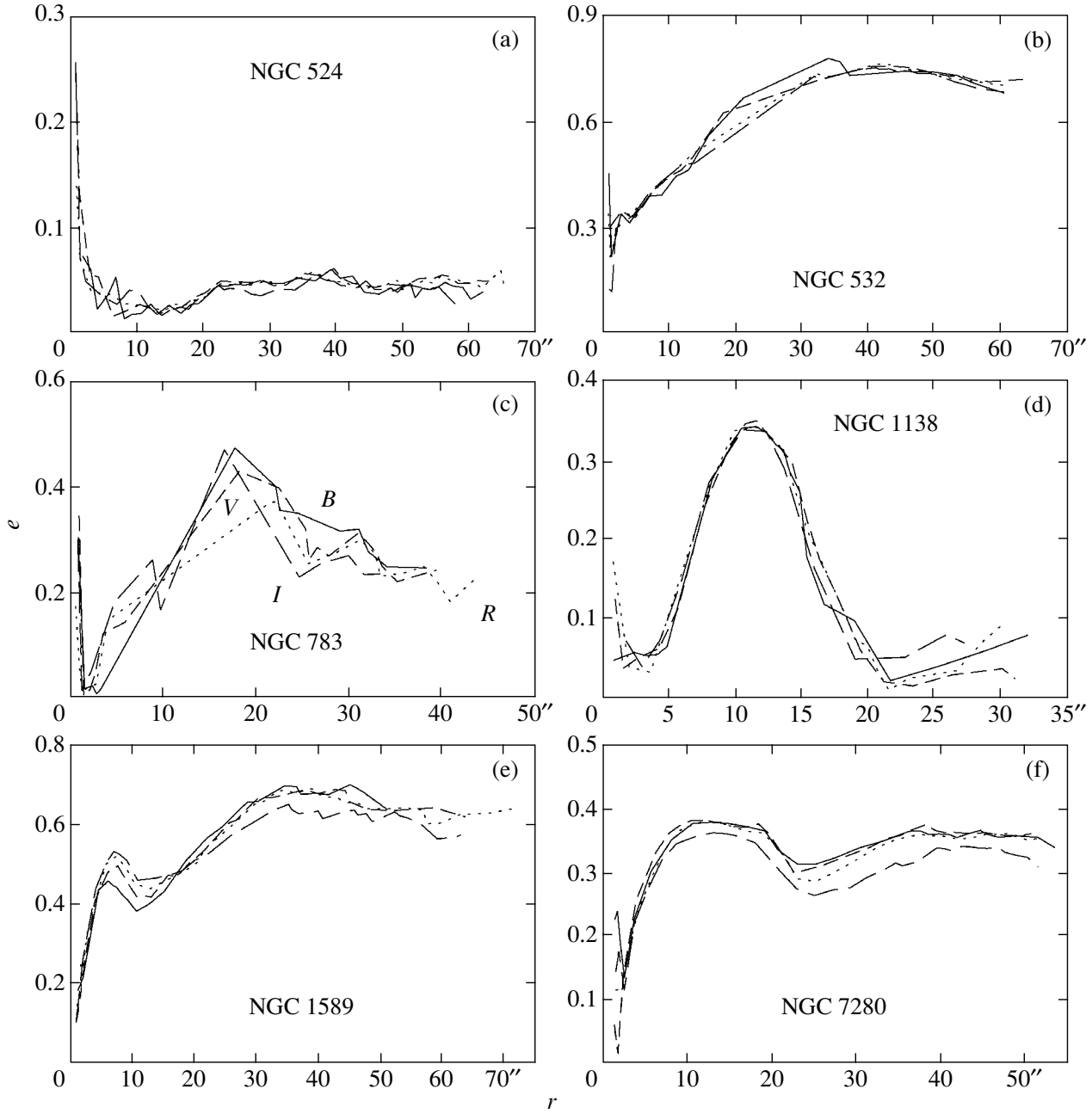

Fig. 2. Same as Fig. 1 for the isophote ellipticity.

ric calibration was 0.06^m in U and B, 0.04^m in V, 0.03^m in R, and 0.02^m in I. The zero-point error for these four galaxies is smaller than the error of the photometric calibration. We estimated the zero-point error for NGC 783 and NGC 1138, for which no aperture photometry is available, to be 0.15^m.

We analyzed the IR properties of the galaxies using the data of the 2MASS-catalog—galaxy images taken in the J, H, and K filters. We reduced these images using a similar procedure. The JHK images have a seeing of $1''$ and a scale of $1.0''/\text{pixel} \times 1.0''/\text{pixel}$.

The sky-background level for the galaxy images is about $24.5^m/\text{arcsec}^2$ in U, $25.0^m/\text{arcsec}^2$ in B, $24.5^m/\text{arcsec}^2$ in V, $23.7^m/\text{arcsec}^2$ in R, $22.5^m/\text{arcsec}^2$ in I, $21.0^m/\text{arcsec}^2$ in J, $20.5^m/\text{arcsec}^2$ in H, and $20.0^m/\text{arcsec}^2$ in K.

We corrected all the data (brightness and color indices) for galactic extinction (based on the LEDA database; Table 1). We assume throughout this paper

a Hubble constant of $H_0 = 75\ \mathrm{km\,s^{-1}\,Mpc^{-1}}$. Given the adopted distances to the galaxies, the image scales are 157, 152, 342, 160, 240, and 126 pc/arcsec for NGC 524, NGC 532, NGC 783, NGC 1138, NGC 1589, and NGC 7280, respectively.

4. ANALYSIS OF THE PHOTOMETRIC RESULTS

4.1. Position Angles and Inclinations of the Galactic Disks

Figures 1a–1f and 2a–2f show the derived position angles (PA) and ellipticities ($e \equiv 1 - b/a$) of the galaxy isophotes in the $UBVRI$ bands at various galactocentric distances. We determined the position angles and inclinations (i) of the galaxies from the outer isophotes in regions where the PA(r) and $e(r)$ dependences flatten. The PA and e values derived from the isophotes in the different bands are generally in good agreement. The only exceptions are the position angles obtained for the disks of NGC 783 and NGC 1138 (Figs. 1c, 1d); this is due to the fact that these galaxies are observed nearly face-on, and NGC 783 has, in addition, a well-developed spiral structure with numerous star-forming regions, which affect the PA(r) and $e(r)$ dependences at short wavelengths.

Table 3 lists our results for the position angles, outer-isophote ellipticities, and inclinations of the galaxies. We calculated the galaxy inclinations using the formula employed in the LEDA database:

$$\cos^2 i = [(b/a)^2 - q_0^2]/(1 - q_0^2), \qquad (1)$$

where $\log q_0 = -0.43 - 0.053\,T$ for $T < 0$ and $q_0 = 0.2$ for $T > 0$, and T is the morphological type of the galaxy.

We analyze the behavior of PA(r) and $e(r)$ in Figs. 1a–1f and 2a–2f in more detail in Section 4.3.

4.2. Averaged Photometric Profiles and Bulge/Disk Decompositions of the Brightness Distributions

We used our position angles and ellipticities for the galactic-disk isophotes to construct averaged $UBVRIJHK$ photometric profiles of the galaxies (Figs. 3a–3f). We performed a bulge/disk decomposition of these profiles by minimizing the difference between the observed profile $I_{\mathrm{obs}}(r)$ and model profile $I_{\mathrm{mod}}(r)$, where $I_{\mathrm{mod}} = I^{\mathrm{b}}(r) + I^{\mathrm{d}}(r)$, using the exponential-disk model

$$I^{\mathrm{d}} = I_0^{\mathrm{d}} \exp(-r/r_0) \qquad (2)$$

Table 3. Position angles and ellipticities of outer isophotes and inclinations of the galactic disks

Galaxy	PA	e	i
NGC 524	$43.7° \pm 1.7°$	0.05 ± 0.01	$20.2° \pm 2.0°$
NGC 532	29.7 ± 0.3	0.74 ± 0.01	80.2 ± 0.9
NGC 783	57.4 ± 1.7	0.25 ± 0.02	42.5 ± 1.2
NGC 1138	28.7 ± 5.1	0.05 ± 0.03	20.9 ± 5.6
NGC 1589	159.5 ± 0.6	0.63 ± 0.01	71.5 ± 0.7
NGC 7280	74.9 ± 1.1	0.36 ± 0.01	57.9 ± 1.0

and a bulge model with the brightness decreasing in accordance with a de Vaucouleurs law:

$$I^{\mathrm{b}} = I_0^{\mathrm{b}} \exp[-(r/r_0)^{1/4}]. \qquad (3)$$

We used the northeastern half of the images of NGC 1589 when constructing the averaged photometric profiles of this strongly inclined galaxy with its powerful dust lanes to the southwest of the major axis (see Fig. 8 below). This enabled us to avoid errors introduced by dust into the derived photometric parameters of the components.

The observed profiles of the central region of NGC 1589 cannot be fit well using a de Vaucoulers bulge with any parameters, but they agree well with an exponential bulge model (Fig. 3e). Lutticke et al. [31] used the law $I^{\mathrm{b}} \sim \exp(-r^{1/2})$ to describe the bulge of NGC 1589.

We now consider certain methodological difficulties in correctly decomposing the one-dimensional photometric profiles of galaxies. One of these concerns the determination of the disk and bulge parameters in ringed galaxies and/or in galaxies with prominent spiral structure. Estimations of the parameters of the components in such galaxies depend strongly on the interval of galactocentric distances r. Due to the presence of relatively bright regions of rings and spirals, formal decompositions yield overestimated disk scales (especially in short-wavelength bands). NGC 783 is the most dramatic example of such a galaxy in our sample (compare Figs. 3c and 3b). Note also the discrepancies between our component parameters for NGC 532 and those derived by Lu [21] (who neglected the spiral arm at $r \approx 45''$) and between our parameters for NGC 524 and NGC 1589 and those of Kent [9, 10] (who neglected bright (or dust) rings in NGC 524 and dust rings and a possible spiral arm in NGC 1589).

The second difficulty concerns the bulge parameters in SB0–SBa galaxies. Averaged photometric profiles include the light of the bar and "spread" this

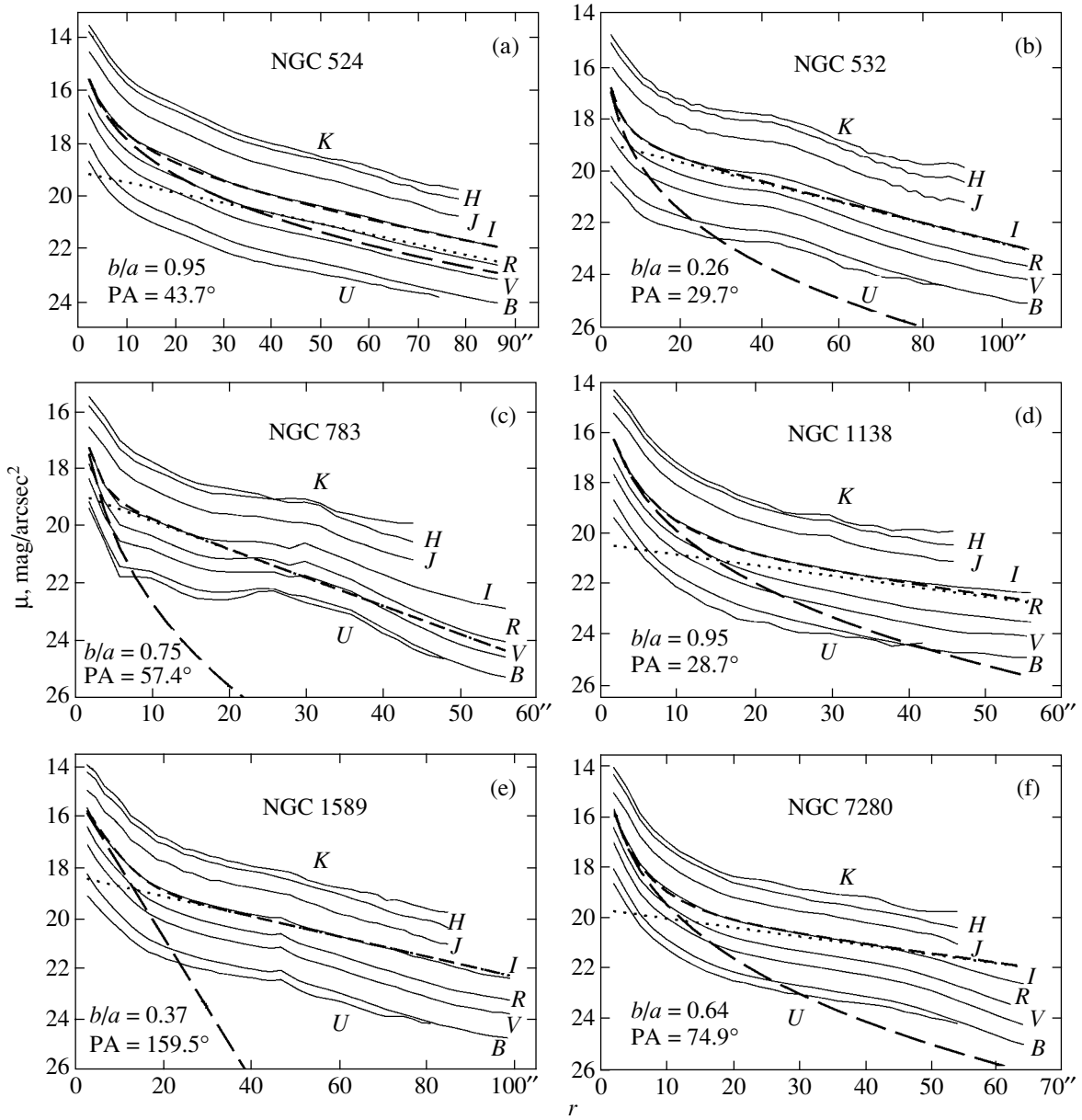

Fig. 3. Averaged photometric profiles of (a) NGC 524, (b) NGC 532, (c) NGC 783, (d) NGC 1138, (e) NGC 1589, and (f) NGC 7280 in the U, B, V, R, I, J, H, and K filters (solid). The model profiles for the bulge (long-dashed) and disk (dotted) and the total model profiles (short-dashed) are also shown for the I filter.

light in azimuth, thereby overestimating the brightness of the bulge. The discrepancies between the model and observed intensity curves for NGC 1138 at $r = 10''-15''$ (Fig. 3d) and for NGC 7280 at $r = 8''-15''$ (Fig. 3f) are due to the allowance for bar radiation in these galaxies.

The effect of bars, rings, spirals, etc. on decompositions of the brightness distribution can be taken into account more correctly by analyzing two-dimensional galaxy images [33]. We refined the model parameters of the bulge and disk (initially derived for the one-dimensional case) using the "mask" method to analyze two-dimensional galaxy images taken in various filters. In this method, the sum of the model disk and bulge images is subtracted from the real galaxy image, $\mu_{\rm obs}(x, y)$; this yields the distribution

$$\mu_m(x, y) = \mu_{\rm obs}(x, y) - \mu_{\rm mod}(x, y), \qquad (4)$$

where

$$\mu_{\rm mod}(x, y) = -2.5 \log [I_{\rm mod}(x, y)] \qquad (5)$$
$$= -2.5 \log [I^{\rm b}(x, y) + I^{\rm d}(x, y)].$$

The resulting "residual" image $\mu_m(x, y)$ is then analyzed. We chose the bulge and disk parameters so

Table 4. Parameters of the galactic disks and bulges

Galaxy	r (disk) r (bulge)	$h^{\rm d}(B)$ $h^{\rm d}(I)$ $h^{\rm d}(K)$	$h^{\rm d}(B)$ $h^{\rm d}(I)$ $h^{\rm d}(K)$, kpc	$\mu_0^{\rm d}(B)$ $\mu_0^{\rm d}(I)$ $\mu_0^{\rm d}(K)$, mag/arcsec^2	$r_{\rm e}^{\rm b}(B)$ $r_{\rm e}^{\rm b}(I)$ $r_{\rm e}^{\rm b}(K)$	$r_{\rm e}^{\rm b}(B)$ $r_{\rm e}^{\rm b}(I)$ $r_{\rm e}^{\rm b}(K)$, kpc	$\mu_{\rm e}^{\rm b}(B)$ $\mu_{\rm e}^{\rm b}(I)$ $\mu_{\rm e}^{\rm b}(K)$, mag/arcsec^2
NGC 524	12″–70″	$27.4'' \pm 1.0''$	4.3 ± 0.2	21.60 ± 0.06	$24.2'' \pm 0.5''$	3.8 ± 0.1	21.88 ± 0.07
	4″–10″	$27.4'' \pm 0.8''$	4.3 ± 0.1	19.14 ± 0.05	$16.4'' \pm 0.8''$	2.6 ± 0.1	18.99 ± 0.18
		$27.0'' \pm 1.5''$	4.2 ± 0.2	17.23 ± 0.09	$15.5'' \pm 0.7''$	2.4 ± 0.1	16.60 ± 0.19
NGC 532	18–94	28.3 ± 0.1	4.3 ± 0.0	21.11 ± 0.01	8.9 ± 3.3	1.4 ± 0.5	22.25 ± 1.47
	4–8	28.1 ± 0.1	4.3 ± 0.0	18.92 ± 0.01	7.8 ± 1.5	1.2 ± 0.2	19.38 ± 0.75
		30.4 ± 0.5	4.6 ± 0.1	17.00 ± 0.03	11.4 ± 2.4	1.7 ± 0.4	17.30 ± 0.87
NGC 783	10–18	13.2 ± 1.3	4.5 ± 0.4	20.87 ± 0.11	–	–	–
	–	11.0 ± 0.3	3.8 ± 0.1	18.79 ± 0.03	–	–	–
		10.7 ± 1.1	3.7 ± 0.4	16.85 ± 0.14	–	–	–
NGC 1138	12–28	28.0 ± 1.4	4.5 ± 0.2	22.85 ± 0.04	4.3 ± 0.1	0.69 ± 0.02	19.84 ± 0.10
	4–8	26.1 ± 1.3	4.2 ± 0.2	20.30 ± 0.05	3.5 ± 0.1	0.57 ± 0.02	17.30 ± 0.12
		28.2 ± 2.5	4.5 ± 0.4	18.53 ± 0.10	3.3 ± 0.1	0.53 ± 0.02	14.65 ± 0.16
NGC 1589	16–38	29.5 ± 0.7	7.1 ± 0.2	20.61 ± 0.02	4.1 ± 0.0	0.99 ± 0.01	17.81 ± 0.03
	0–16	27.2 ± 0.5	6.5 ± 0.1	18.31 ± 0.02	3.8 ± 0.1	0.92 ± 0.02	15.21 ± 0.05
		24.6 ± 0.8	5.9 ± 0.2	16.24 ± 0.04	4.1 ± 0.1	0.99 ± 0.03	13.33 ± 0.10
NGC 7280	12–38	37.1 ± 1.6	4.7 ± 0.2	22.06 ± 0.03	4.1 ± 0.5	0.52 ± 0.06	19.21 ± 0.49
	4–8	30.5 ± 1.1	3.8 ± 0.1	19.70 ± 0.03	3.0 ± 0.5	0.38 ± 0.06	16.61 ± 0.67
		33.0 ± 1.9	4.2 ± 0.2	18.02 ± 0.07	2.3 ± 0.4	0.29 ± 0.06	13.79 ± 0.90

as to make the values of the image pixels $\mu_m(x, y)$ outside bars, rings, and spiral arms close to zero.

Table 4 lists the resulting model parameters for the disks (scale length $h^{\rm d}$ and central surface brightness $\mu_0^{\rm d}$) and bulges (effective radius $r_{\rm e}^{\rm b}$ and brightness $\mu_{\rm e}^{\rm b} \equiv \mu^{\rm b}(r_{\rm e})$) in the B, I, and K bands together with the range of galactocentric distances r where the modeling was performed. The bulge contribution to the total light of the late-type galaxy NGC 783 is extremely small. We included it formally when constructing the model profiles of the galaxy, but do not list the corresponding bulge parameters in Table 4. For NGC 1589, which has an exponential bulge, Table 4 lists the radial scale length and the central brightness of the bulge ($h^{\rm b}$ and $\mu_0^{\rm b}$, respectively).

Note that the ratios $h^{\rm d}(I)/D_{25}^0$ for four giant galaxies with $D_{25}^0 > 30$ kpc lie within the narrow interval from 0.12 to 0.14, whereas the relatively small galaxies NGC 1138 and NGC 7280 have $h^{\rm d}/D_{25}^0 = 0.23$–$0.24$ (Tables 1, 4). These data agree well with the results of Elmegreen and Elmegreen [42], but more extensive samples of galaxies of various sizes, inclinations, and morphological types are required for a more complete analysis and interpretation of the behavior of $h^{\rm d}(I)/D_{25}^0$.

Figures 4–9 show the residual galaxy images μ_m. Since the decompositions did not include the nuclear regions of the galaxies ($r \leq 2''$), the brightness and color of these regions in Figs. 4–9 are formally reduced to the brightness and color of the surrounding circumnuclear regions.

4.3. Specific Features of the Galaxies' Structure

The galaxy images $\mu_m(x, y)$ obtained by subtracting the disk and bulge brightness fields from the real galaxy in accordance with (4) and (5) can be used to identify and analyze a number of subtle morphological features that are inconspicuous in the galaxy images.

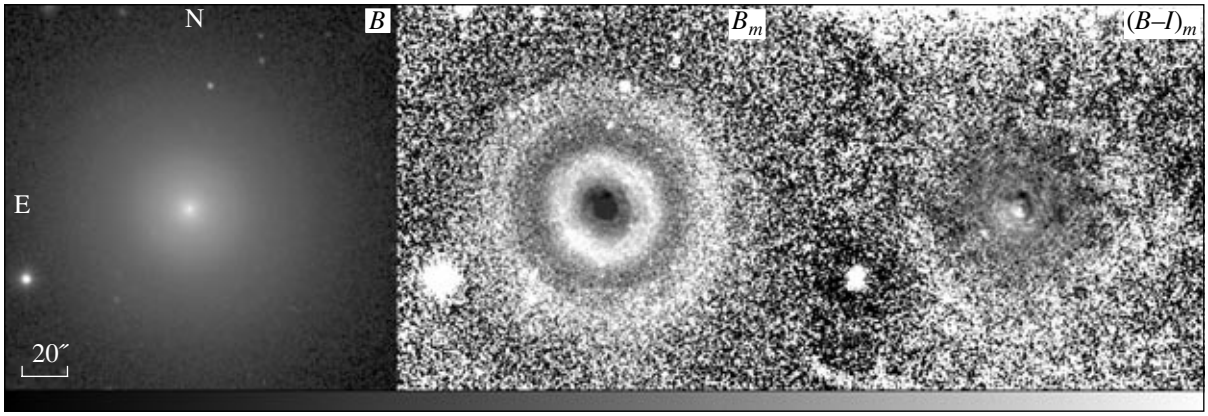

Fig. 4. B image of NGC 524 (left), "residual" image B_m (center), and map of the "residual" color index $(B–I)_m$ (right). The range of brightness values (from black to white) is $B = 27^m/\text{arcsec}^2 \ldots 17^m/\text{arcsec}^2$, $B_m = 0.2^m/\text{arcsec}^2 \ldots -0.2^m/\text{arcsec}^2$, $(B–I)_m = 0.1^m \ldots -0.1^m$. The image scales are also shown.

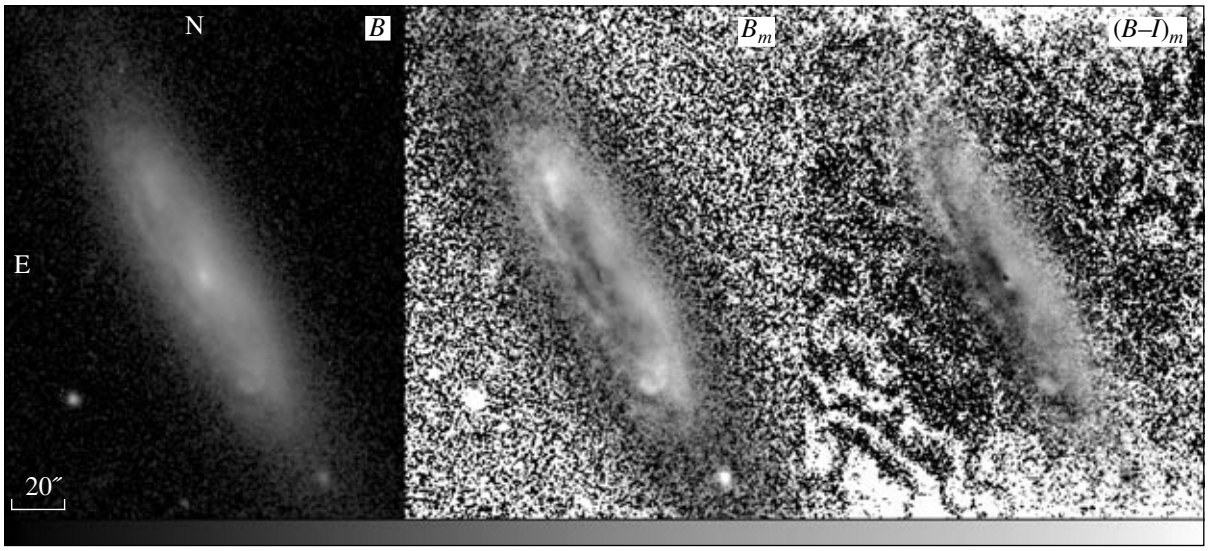

Fig. 5. Same as Fig. 4 for NGC 532. The range of brightness values (from black to white) is $B = 26^m/\text{arcsec}^2 \ldots 18^m/\text{arcsec}^2$, $B_m = 1^m/\text{arcsec}^2 \ldots -1^m/\text{arcsec}^2$, $(B–I)_m = 0.5^m \ldots -0.5^m$.

Figures 4–9 show the B galaxy images (left), the residual images B_m (center), and maps of the residual color index $(B–I)_m$ (right), where

$$B_m = B_{\text{obs}} - B_{\text{mod}}, \quad (6)$$

$$(B–I)_m = (B_{\text{obs}} - B_{\text{mod}}) - (I_{\text{obs}} - I_{\text{mod}}). \quad (7)$$

Let us consider each galaxy separately.

NGC 524. This "classical" lenticular galaxy exhibits radial brightness variations (with an amplitude of up to 0.2^m), with a relative brightness excess at $r = 15''–25''$ and $r = 50''–60''$ and/or relatively low brightness at $r = 30''–40''$ and $r = 70''–80''$ (Fig. 4). This is clearly a galaxy with two stellar rings or two dark dust rings. Modeling of the bulge and disk parameters admits either of these possibilities. Harris and Hanes [5] and Veron-Cetty and Veron [8] believe that the dark rings contain dust; however, we found no differences in the $(B–I)_m$ color between the dark and bright rings (Fig. 4). The disk and bulge parameters in Fig. 3a and Table 4 are based on the assumption that the galaxy contains two bright stellar rings.

Correct interpretation of the brightness variations in NGC 524 requires a detailed analysis of the kinematics of the galaxy and determination of the radii of the Lindblad resonances and the corotation resonance. In their analysis of the brightness distribution in NGC 524 out to a galactocentric distance of 140″, Baggett et al. [7] found that brightness variations per-

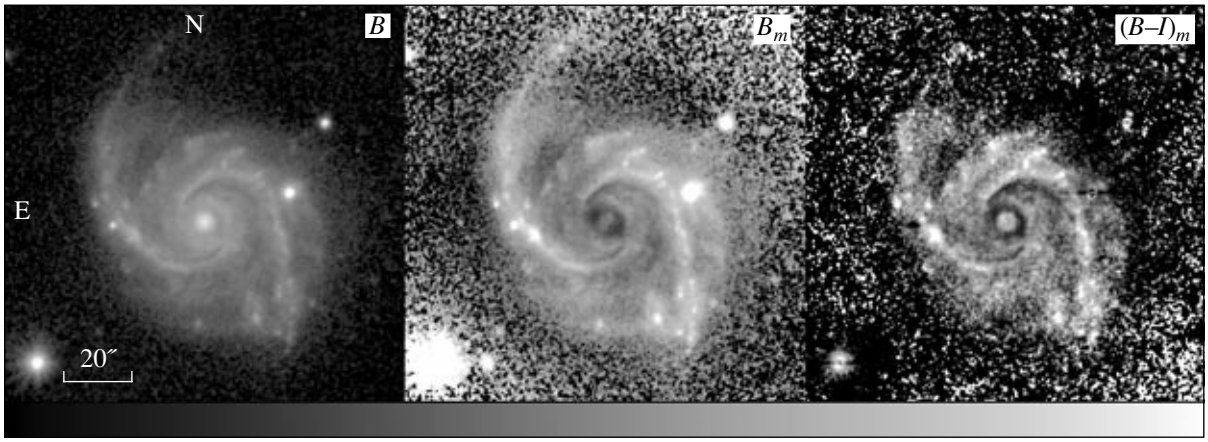

Fig. 6. Same as Fig. 4 for NGC 783. The range of brightness values (from black to white) is $B = 26^m/\text{arcsec}^2 \ldots 18^m/\text{arcsec}^2$, $B_m = 2^m/\text{arcsec}^2 \ldots -2^m/\text{arcsec}^2$, $(B-I)_m = 0.6^m \ldots -0.6^m$.

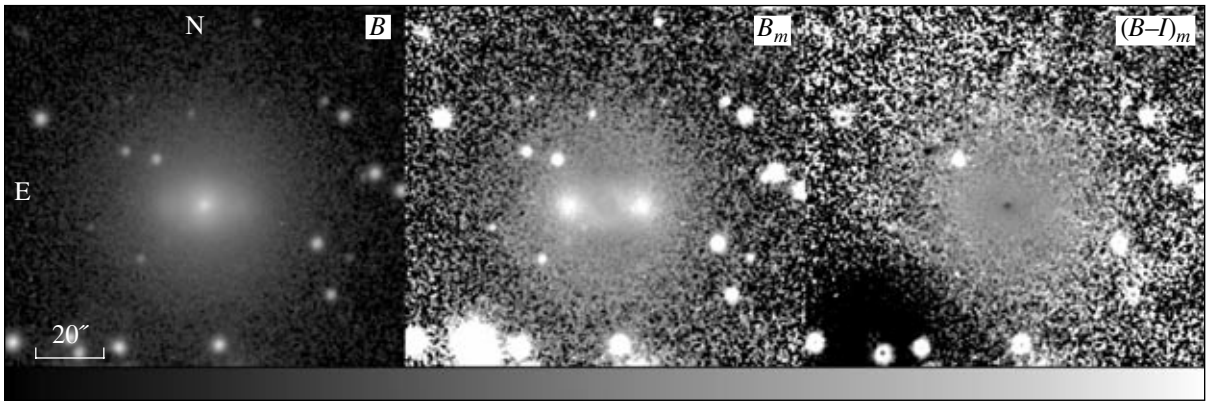

Fig. 7. Same as Fig. 4 for NGC 1138. The range of brightness values (from black to white) is $B = 26^m/\text{arcsec}^2 \ldots 17^m/\text{arcsec}^2$, $B_m = 1.5^m/\text{arcsec}^2 \ldots -1.5^m/\text{arcsec}^2$, $(B-I)_m = 0.6^m \ldots -0.6^m$.

sist in the outer regions (in particular, the galaxy displays a relative brightness excess at $r = 120''-130''$).

Galaxy rings affect the PA(r) and $e(r)$ dependences (Figs. 1a, 2a). On the whole, the PA and e values remain constant with radius in NGC 524, however, a local minimum of the PA ($\approx 35°$) and isophote ellipticity ($e = 0.025$) can be seen at $r = 15''-18''$ (the inner part of the first bright ring) and a local maximum (PA $= 50°$, $e = 0.07$) at $r \approx 40''$ (the outer part of the first dark ring). The inner regions in NGC 524 ($r < 15''$) are less spherically symmetric (Fig. 4): the brightness distribution shows a PA jump to 50° (at $r = 7''-8''$), with e decreasing from 0.1 down to 0.03 (Figs. 1a, 2a). The variations of the position angle and ellipticity of isophotes in the inner region of NGC 524 are most likely due to dust lanes [6, 15]. The spherically symmetric bulge dominates at $r \sim 10''-20''$ (minimum e values), whereas the disk light begins to show up at greater galactocentric distances. The PA(r) and $e(r)$ dependences flatten at $r > 40''$ (Figs. 1a, 2a), where the brightness distribution is dominated by the disk (Fig. 3a).

NGC 532. The inner structure of the galaxy is barely discernible in the B filter (Fig. 5). However, the B_m and $(B-I)_m$ residual images show a bright half-ring in the northwestern part of the galaxy—the region of spiral arms at $r \approx 40''-60''$, with local bright fragments (B_m to -0.7^m). Although the spiral is less conspicuous in the southeastern half of the galaxy, we can identify two dark dust lanes ($(B-I)_m \geq 0.3^m$): the inner dust lane (at a deprojected distance $r \approx 5''-10''$) and an outer dust lane that goes along the inner edge of the spiral (Fig. 5).

NGC 532 exhibits gradients of the brightness ($B_m \approx -0.2^m-0.2^m$) and color ($(B-I)_m \approx -0.1^m-0.1^m$) along its minor axis (Fig. 5). The southeastern (farther) part of the galaxy appears redder and fainter. In strongly inclined galaxies, such a brightness distribution is suggestive of an optically thick dust disk, consistent with the data of

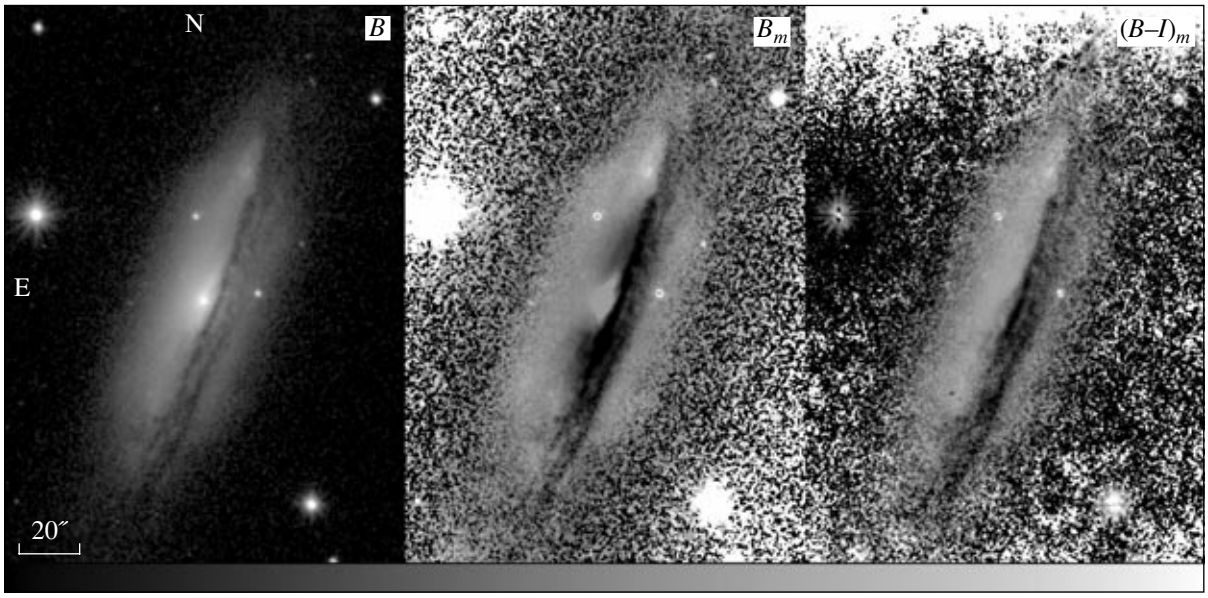

Fig. 8. Same as Fig. 4 for NGC 1589. The range of brightness values (from black to white) is $B = 25^m/\text{arcsec}^2 \ldots 18^m/\text{arcsec}^2$, $B_m = 1.5^m/\text{arcsec}^2 \ldots -1.5^m/\text{arcsec}^2$, $(B–I)_m = 1^m \ldots -1^m$.

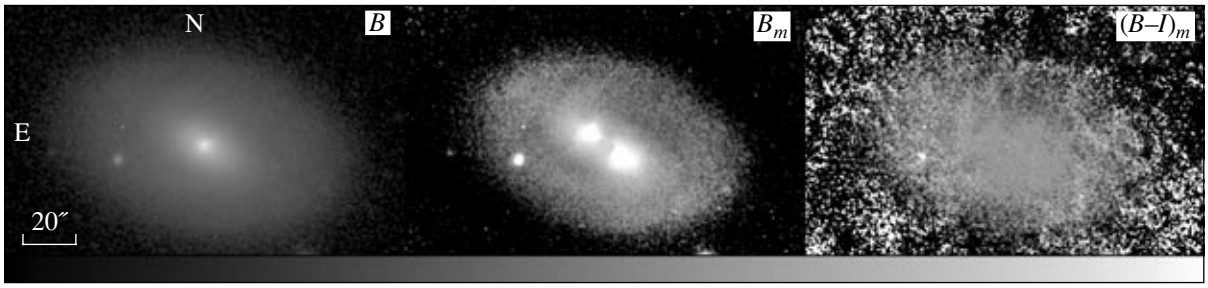

Fig. 9. Same as Fig. 4 for NGC 7280. The range of brightness values (from black to white) is $B = 26^m/\text{arcsec}^2 \ldots 17^m/\text{arcsec}^2$, $B_m = 0.75^m/\text{arcsec}^2 \ldots -0.75^m/\text{arcsec}^2$, $(B–I)_m = 0.5^m \ldots -0.5^m$.

Bettoni et al. [24] indicating a large mass of dust in NGC 532.

The position angle of the isophotes remains constant at $r > 10''$ (Fig. 1b) in the region dominated by the disk brightness (Fig. 3b). The isophote ellipticity varies more smoothly: $e(r)$ flattens in the region of the spiral arms (at $r > 30''$). On the whole, the variations of PA(r) and $e(r)$ reflect the increase of the disk brightness contribution with increasing galactocentric distance. The observed parameters of the bulge isophotes are PA $\approx 22°$, $e \approx 0.3$ (Figs. 1b, 2b), while the parameters of the galactic disk are PA $\approx 30°$, $e \approx 0.75$ (Table 3).

NGC 783. This galaxy is the only late-type spiral in our sample, and has a complex structure (Fig. 6). The spherical component can be traced to $r \approx 5''$ (Figs. 1c, 2c, 3c, 6). The bulge isophotes are almost circular ($e \approx 0.03$). A ring can be seen at a galactocentric distance of $r = 8''$ (Fig. 6). The ellipticity ($\sim$0.3) and position angle ($\sim 60°$) of the isophotes of this ring almost coincide with the PA and e values for the galactic disk (Table 3).

The B_m image of NGC 783 shows a structure resembling a circumnuclear bar in the inner part of the galaxy. It has boxy isophotes with apparent semiaxes of $3.5''$ by $1.8''$ (the deprojected size is $\sim 5'' \times 2''$) and a position angle of 145°. However, we cannot be completely sure that NGC 783 has a circumnuclear bar: the triaxial structure stands out against the spherical component at $r = 2''–3.5''$, where it exceeds only slightly the angular resolution of galaxy images (Table 2). The arrangement of the "bar" along the minor axis of NGC 783 also raises some doubts: such a structure in the B_m residual image could develop artificially due to incorrect determination of bulge isophote ellipticity. On the other hand, the position angle of galaxy isophotes peaks (170°) just at $r = 4''$ (Fig. 1c). Moreover, active star formation is occurring

in the nucleus of NGC 783 [26]. Star-formation processes in galactic nuclei are often stimulated by bars (classical or circumnuclear) along which gas moves toward the nucleus.

Two symmetric, weakly wound branching spiral arms with numerous star-forming regions begin at distances $r = 8''-12''$ (Fig. 6). The spiral arms are prominent against the surrounding disk, in both brightness ($B_m \approx -1.4^m$) and color ($(B-I)_m \approx -0.4^m$). Dust lanes can be seen along the inner edges of the arms north and south of the center of NGC 783 (Fig. 6). These dust lanes are especially prominent in the color image: $(B-I)_m \approx 0.4^m$. Two short, weak arms can be seen about $7''-9''$ to the north and south of the spiral arms of the galaxy (Fig. 6). The spiral structure can be traced to $r \sim 40''$.

Note that, although the model profile of the galaxy differs strongly from the profile observed in Fig. 3c, the residual disk brightness outside the spiral arms is $B_m = \pm 0.1^m$ (Fig. 6).

The position angle and ellipticity of the isophotes remain constant in the region of the spiral arms ($r \geq 25''$) (Figs. 1c, 2c). The maximum isophote ellipticity (to 0.48) at $r = 17''$ (Fig. 2c) is due to the emergence of two bright symmetric isophotes at this distance, which "extend" the galaxy isophotes.

NGC 1138. This galaxy is viewed face-on, and has a fairly simple structure. Three components can be identified: the bulge, bar, and disk. Although the bar is barely discernible in the B band, and can be seen only due to the variation of the ellipticity of the isophotes at $r = 8''-15''$ (Fig. 2d), the B_m residual image shows a classical "flat" bar (according to the classification of Elmegreen and Elmegreen [43]) (Fig. 7). The bar isophotes have an almost boxy shape, with semiaxes $\sim 18'' \times 8''$ ($e = 0.66 \pm 0.01$). The position angle of the bar is PA $= 89.8° \pm 0.4°$ (Fig. 1d), i.e., it is oriented almost exactly East–West. The bar's brightness exceeds the brightness of the surrounding background by $0.6^m-0.9^m$ (in the B_m image). The bar does not stand out against the bulge and disk in terms of its color parameters. On the whole, the galaxy appears fairly uniform in the $(B-I)_m$ residual color image (Fig. 7). There is a small color gradient (from 0.2^m to -0.2^m) with radius, due to the increasing contribution of the disk to the total light of NGC 1138 with increasing galactocentric distance.

The bar is located in the region dominated by the light of the spherical component. The disk provides the main contribution to the brightness at $r \geq 20''$. The B surface brightness does not exceed $23^m/\text{arcsec}^2$ at these distances (Fig. 3d). The disk isophotes are almost circular, $e = 0.05$, and the position angle of the outer isophotes is inferred with a large uncertainty (Fig. 1d).

NGC 1589. This strongly inclined galaxy shows powerful dust lanes. The B and B_m images show two well-defined dark lanes: one at a deprojected distance of $r = 16''$ (B_m to 1.8^m) and a second, weaker lane at $r = 31''$ (B_m to 0.7^m; Fig. 8). However, the sharp lane boundaries appear blurred in the $(B-I)_m$ image, where we see instead a thick line of dust mixed with stars and gas. Jansen et al. [28] explain the "double" appearance of the dust lane in NGC 1589 by the presence of a spiral arm. In this case, the thickness of the dust disk is $9''$, which corresponds to a deprojected size of $28''$ (6.8 kpc), and the thickness of the spiral arm is $2''$ (observed) or $6''$ (1.5 kpc, deprojected). The spiral arm in the dust disk can be seen at deprojected distances of $\sim 25''-38''$. Spiral-arm elements in the farther (eastern) part of NGC 1589 are located at distances of $r = 40''-50''$. We can see two blue ($(B-I)_m$ to -0.6^m) regions of enhanced brightness (with B_m ranging to -1.1^m), one to the north of the nucleus and another, fainter region to the southeast of the nucleus (Fig. 8). In the framework of the hypothesis of Jansen et al. [28], the observed shape of NGC 1589 suggests that the galaxy has a thick but relatively small stellar and gaseous disk and spiral arms. In the western part of the galaxy, we see the inner part of the arm as a bright band between two dust lanes. The outer regions of the spiral arm are superimposed on the outer part of the dust disk (i.e., the farthest part). The brightness difference between the inner and outer parts of the dust disk ($B_m = 1.8^m - 0.7^m = 1.1^m$) can be explained by the effect of the spiral arm.

The bulge of NGC 1589 shows up prominently at $r \leq 15''$ in the B_m image (Fig. 8). The shape of the bulge isophotes differs from elliptical, but the observed asymmetry of the bulge can easily be explained by extinction in the thick dust disk of the galaxy (west of the center) and, in our opinion, is not physically real (as also suggested by Lutticke et al. [31]).

The presence of dust has a strong effect on the ellipticity of the isophotes, including those in the central region, which is dominated by the radiation of the bulge. The thick dust disk distorts the shapes of the isophotes at $r > 10''$. The local maximum of $e(r)$ at $r = 5''$ (Fig. 2e) is also probably associated with the weak dust lane.

The presence of a bar in NGC 1589 was noted in [31]. However, we could not find any evidence for a bar in NGC 1589 either visually or in the behavior of $e(r)$.

On the whole, NGC 1589 morphologically resembles NGC 532. The only important difference between

these two galaxies is the presence of a powerful dust disk in NGC 1589.

NGC 7280. The structure of NGC 7280 is almost identical to that of NGC 1138, but the former has been studied much more thoroughly. Like in NGC 1138, the bar in NGC 7280 can be seen visually only via the variation of the isophote position angle. Our results for the parameters of the bar and disk agree well with those obtained by Erwin and Sparke [34] and Erwin [37]: the position angles of the disk are PA $= 74.9° \pm 1.1°$ and $72°-73°$, and the disk isophote ellipticities $e = 0.36 \pm 0.01$ and 0.33, according to our data and [34, 37], respectively (Figs. 1f, 2f). The (undeprojected) position angles of the bar are $62.6° \pm 0.4°$ and 63°, and the isophote ellipticities $e = 0.38 \pm 0.01$ and 0.40, according to our data and [34], respectively. Our semimajor axis for the bar (21″) is also similar to that found by Erwin [34]. The brightness of the bar (based on the B_m image) exceeds the level of the surrounding background by $0.2^m-0.9^m$. The bar does not stand out against the bulge or disk in terms of its color parameters (Fig. 9).

The bar of NGC 7280 is turned only 12° with respect to the major axis of the galactic disk, and the ellipticity of the bar isophotes is almost the same as that of the disk isophotes. This is why PA and e vary only slightly with radius (Figs. 1f, 2f). The eccentricity reaches its minimum, $e = 0.3$, at $r = 23''$ (Fig. 2f), just beyond the tip of the bar. This behavior of $e(r)$ can be explained by the substantial contribution of the brightness of the spherical component at this radius (Fig. 3f).

The galaxy exhibits small gradients in the brightness (from 0.15^m to -0.15^m in B_m) and color (from 0.1^m to -0.1^m in $(B-I)_m$) along its minor axis. The southeastern part of the galaxy (which is brighter and bluer) is closer to us. As in NGC 532, such a gradient can be explained by the presence of an optically thick dust disk. The other possible explanation, that there is a dust disk with a similar position angle for its major axis inclined to the stellar disk, is less likely.

The galaxy has two very faint spiral arms (with B_m not exceeding -0.2^m) emerging from the tips of the bar (Fig. 9). The direction of winding of the spiral arms and the kinematics of the stars in the circumnuclear disk (according to the results of Afanasiev and Sil'chenko [35]) lead us to conclude that NGC 7280 rotates in the counterclockwise direction, as was suggested earlier by Erwin and Sparke [34].

5. CONCLUSIONS

We have reported here the results of multicolor surface photometry of six lenticular and spiral galaxies. These are the first multicolor CCD photometric data for three of the galaxies (NGC 532, NGC 783, and NGC 1138).

We have analyzed the overall structure of the galaxies and performed a bulge/disk decomposition of the galaxy images.

We have analyzed the structure of the galaxies and refined the model parameters describing the disk and bulge using the "mask" method, in which the sum of the model images for the disk and bulge is subtracted from the galaxy image and the resulting residual image analyzed.

The main results of this paper include the following.

(1) NGC 524 shows radial brightness variations that can be explained by the presence of two stellar and/or dust rings in the galaxy. We determined the positions of spiral arms in NGC 532, NGC 1589, and NGC 7280. We found a ring in the central part of NGC 783, and suspect the presence of a circumnuclear bar. We determined the parameters of the bars in NGC 1138 and NGC 7280; the bars in both galaxies have flat brightness profiles along the major axis.

(2) The brightness decrease in the bulge of NGC 1589 is described fairly well by an exponential law, whereas the brightness decreases in other galaxies with prominent bulges agrees with a de Vaucouleurs law.

(3) We confirm the conclusion of Erwin and Sparke [34] that NGC 7280 rotates in the counterclockwise direction.

(4) Five galaxies show photometric evidence of dust: NGC 1589 exhibits a thick dust disk, NGC 532 and NGC 7280 have "semitransparent" disks, NGC 524 may contain dust rings, and dust lanes can be seen along the inner edges of the spiral arms in NGC 532 and NGC 783.

(5) Our estimates for the relative disk scale heights $h^{\rm d}(I)/D^0_{25}$ for the four giant galaxies with diameters $D^0_{25} > 30$ kpc lie in the interval from 0.12 to 0.14.

(6) The bulge/disk decompositions of the one-dimensional averaged photometric profiles of barred and ringed galaxies with well-developed spiral structure often yield incorrect parameters for the bulge and disk. The decomposition of the brightness distribution in such galaxies should be performed using two-dimensional images.

ACKNOWLEDGMENTS

I am grateful to A.V. Zasov (Sternberg Astronomical Institute) for fruitful discussions of this work and assistance with the selection of objects for photometry, and to S.I. Ponomarenko (Sternberg Astronomical Institute) and the staff of the Ulugh Bek Astronomical Institute of the Academy of Sciences of the Republic of Uzbekistan for assistance in the observations. This work was supported by the Russian Foundation for Basic Research (project nos. 04-02-16518 and 05-02-16454).

REFERENCES

1. F. Simien and Ph. Prugniel, Astron. Astrophys. **384**, 371 (2002).
2. R. Buta and K. L. Williams, Astron. J. **109**, 543 (1995).
3. S. S. Larsen, J. P. Brodie, J. P. Huchra, et al., Astron. J. **121**, 2974 (2001).
4. M. J. Geller and J. P. Huchra, Astrophys. J., Suppl. Ser. **52**, 61 (1983).
5. W. E. Harris and D. A. Hanes, Astrophys. J. **291**, 147 (1985).
6. J. Kormendy, Astrophys. J. **292**, L9 (1985).
7. W. E. Baggett, S. M. Baggett, and K. S. J. Anderson, Astron. J. **116**, 1626 (1998).
8. M.-P. Veron-Cetty and P. Veron, Astron. Astrophys. **204**, 28 (1988).
9. S. M. Kent, Astrophys. J., Suppl. Ser. **59**, 115 (1985).
10. S. M. Kent, Astrophys. J., Suppl. Ser. **121**, 2974 (2001).
11. O. K. Sil'chenko, Astron. J. **120**, 741 (2000).
12. M. A. Beasley, D. A. Forbes, J. P. Brodie, and M. Kissler-Patig, Mon. Not. R. Astron. Soc. **347**, 1150 (2004).
13. P. Jablonka, P. Martin, and N. Arimoto, Astron. J. **112**, 1415 (1996).
14. H. R. Schmitt, Astron. J. **122**, 2243 (2001).
15. F. Schweizer and P. Seitzer, Astron. J. **104**, 1039 (1992).
16. S. F. Helsdon, T. J. Ponman, E. O'Sullivan, and D. A. Forbes, Mon. Not. R. Astron. Soc. **325**, 693 (2001).
17. T. X. Thuan and M. Sauvage, Astron. Astrophys., Suppl. Ser. **92**, 749 (1992).
18. N. Caldwell, R. Kennicutt, and R. Schommer, Astron. J. **108**, 1186 (1994).
19. F. Macchetto, M. Pastoriza, N. Caon, et al., Astron. Astrophys., Suppl. Ser. **120**, 463 (1996).
20. Ph. Heraudeau and F. Simien, Astron. Astrophys., Suppl. Ser. **118**, 111 (1996).
21. N. Y. Lu, Astrophys. J. **506**, 673 (1998).
22. Ph. Prugniel, G. Maubon, and F. Simien, Astron. Astrophys. **366**, 68 (2001).
23. R. Lutticke, R.-J. Dettmar, and M. Pohlen, Astron. Astrophys., Suppl. Ser. **145**, 405 (2000).
24. D. Bettoni, G. Galletta, and S. Garcia-Burillo, Astron. Astrophys. **405**, 5 (2003).
25. G. Moriondo, C. Baffa, S. Casertano, et al., Astron. Astrophys., Suppl. Ser. **137**, 101 (1999).
26. T. Contini, S. Considere, and E. Davoust, Astron. Astrophys., Suppl. Ser. **130**, 285 (1998).
27. C. Magri, Astron. J. **108**, 896 (1994).
28. R. A. Jansen, J. H. Knapen, J. E. Beckman, et al., Mon. Not. R. Astron. Soc. **270**, 373 (1994).
29. L. E. Kuchinski and D. M. Terndrup, Astron. J. **111**, 1073 (1996).
30. L. E. Kuchinski, D. M. Terndrup, K. D. Gordon, and A. N. Witt, Astron. J. **115**, 1438 (1998).
31. R. Lutticke, M. Pohlen, and R.-J. Dettmar, Astron. Astrophys. **417**, 527 (2004).
32. M. V. Alonso, M. Bernardi, L. N. da Costa, et al., Astron. J. **125**, 2307 (2003).
33. R. E. de Souza, D. A. Gadotti, and S. dos Anjos, Astrophys. J., Suppl. Ser. **153**, 411 (2004).
34. P. Erwin and L. S. Sparke, Astrophys. J., Suppl. Ser. **146**, 299 (2003).
35. V. L. Afanasiev and O. K. Sil'chenko, Astron. J. **119**, 126 (2000).
36. N. Caldwell, J. A. Rose, and K. D. Concannon, Astron. J. **125**, 2891 (2003).
37. P. Erwin, Astron. Astrophys. **415**, 941 (2004).
38. W. van Driel and H. van Woerden, Astron. Astrophys. **243**, 71 (1991).
39. B. P. Artamonov, Yu. Yu. Badan, V. V. Bruevich, and A. S. Gusev, Astron. Zh. **76**, 438 (1999) [Astron. Rep. **43**, 377 (1999)].
40. A. U. Landolt, Astron. J. **104**, 340 (1992).
41. G. Petrov, W. Seggewiss, A. Dieball, and B. Kovachev, Astron. Astrophys. **376**, 745 (2001).
42. D. M. Elmegreen and B. G. Elmegreen, Astrophys. J., Suppl. Ser. **54**, 127 (1984).
43. B. G. Elmegreen and D. M. Elmegreen, Astrophys. J. **288**, 438 (1985).

Translated by A. Dambis